

Instead of conclusions

The research on saturation/CGC physics is ongoing, with a number of open theoretical and phenomenological questions. Therefore, instead of conclusions, in this chapter we briefly review the phenomenology of saturation/CGC physics and list some important open theoretical problems.

9.1 Comparison with experimental data

In this section we will give a brief overview of how high energy QCD theory compares with the current experimental data. The reader may wonder whether such a comparison is possible to fit into one short section; indeed, a comparison of saturation/CGC physics with experiment could be a subject for a separate book. However, a serious quantitative comparison with experiment suffers from two major difficulties. The first is that a well-developed theoretical approach exists only for the scattering of a dilute parton system on a dense one; the key examples are DIS on nuclei (eA) and the proton–nucleus (pA) collisions considered earlier. At the same time, much of the data exist either for the scattering of a dense parton system on another dense parton system, as is the case in nucleus–nucleus (AA) collisions, or for the scattering of two dilute systems on each other, like DIS on a proton (ep) or proton–proton (pp) collisions. The theoretical progress in the description of these reactions in the saturation/CGC framework is rather limited, with many open questions and opportunities for further research (see Sec. 8.3 for a brief summary of the existing AA results). Hence, in describing the AA , ep , and pp data using existing theoretical knowledge one is often forced to make assumptions whose validity is hard to verify.

The second difficulty in comparing the saturation/CGC physics with experiment is in the fact that many experimental observations allow alternative descriptions, usually in the framework of DGLAP evolution within the standard collinear factorization framework. The key problem is that an *experimentum crucis* that would allow us to unambiguously differentiate the nonlinear saturation physics from the linear DGLAP evolution has not been found. This is also partly a theoretical problem.

On the positive side, high energy QCD leads to a unified description of various experimental observations providing not only a possible understanding of the underlying physics but also suggestions and directions for future experiments. The phenomenological picture

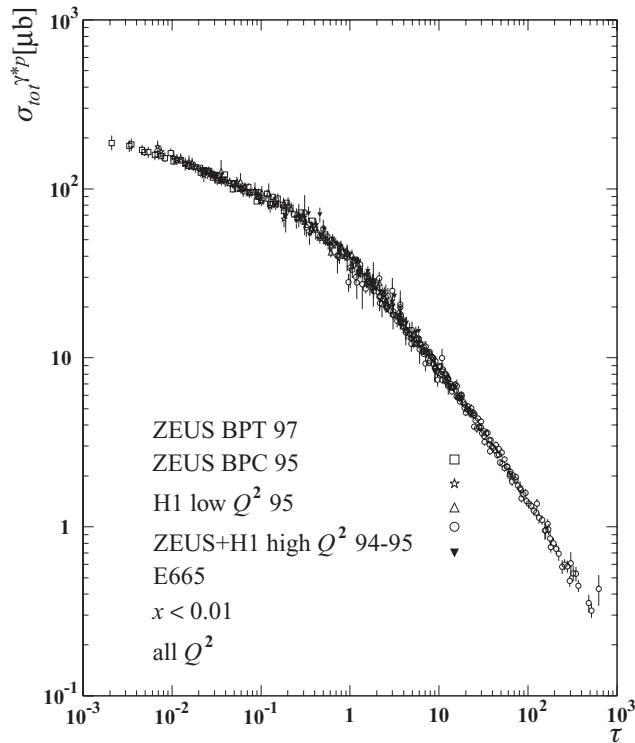


Fig. 9.1. Geometric scaling in the total γ^*p cross section in DIS. (Reprinted with permission from Stasto, Golec-Biernat, and Kwiecinski (2001). Copyright 2001 by the American Physical Society.)

resulting from the theoretical developments discussed in this book is so beautiful, universal, and self-consistent that we cannot finish the book without sharing it with our reader.

9.1.1 Deep inelastic scattering

As discussed earlier (see Sec. 4.5), one of the most striking predictions of high energy QCD is that the DIS structure functions should depend on only one variable, $\tau = Q^2/Q_s^2$: this is the phenomenon of *geometric scaling*. This scaling behavior is a manifestation of the simple idea that the only relevant dimensionful scale at high energy is the saturation momentum. Geometric scaling was first observed by Stasto, Golec-Biernat, and Kwiecinski (2001) and is shown in Fig. 9.1 for a compilation of HERA data on the total γ^*p cross section for $x < 0.01$.

Another important consequence of saturation physics is that the ratio of the diffractive and total cross sections should be independent of energy (see Eqs. (7.23) and the discussion around them). The experimental data from HERA shown in Fig. 9.2 appears to agree with this prediction.

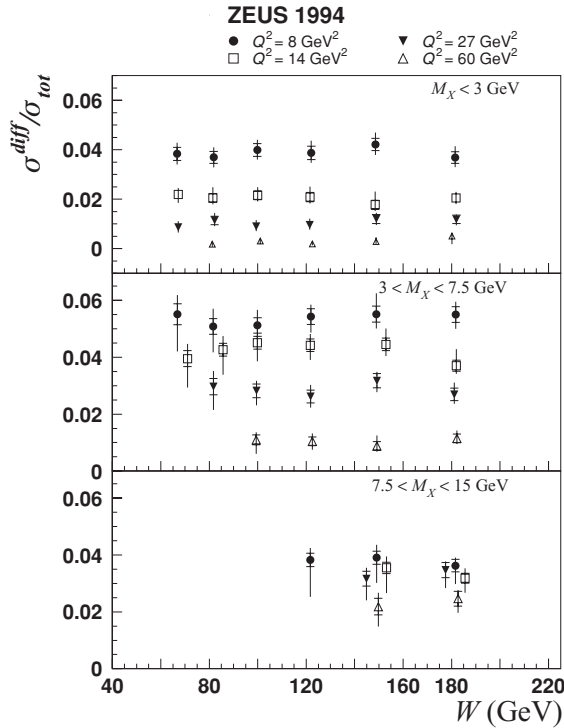


Fig. 9.2. The ratio of the cross section for diffractive production in DIS and the total cross section, as a function of energy W , for different intervals in the mass of the produced hadrons M_X . (Reprinted with permission from Abramowicz and Caldwell (1999). Copyright 1999 by the American Physical Society.)

On the more quantitative side, the first comprehensive fit of the HERA DIS data based on a variation of the GGM/MV formula (4.51) for the dipole amplitude was carried out by Golec-Biernat and Wusthoff (1999a, b) and is known as the GBW model (see Eqs. (4.12), (4.24), and (4.10) for the relation between F_2 , F_1 , and the dipole amplitude N). A more recent fit, based on rcBK evolution, of the combined data on the DIS cross section reported by the H1 and ZEUS experiments at HERA is shown in Fig. 9.3. It can be seen that the “reduced” DIS cross section, defined by

$$\sigma_r = F_2 - \frac{y^2}{1 + (1 - y)^2} F_L \tag{9.1}$$

(with y from Eq. (2.2)) is well described by the rcBK evolution.

9.1.2 Proton(deuteron)–nucleus collisions

The formalism developed in this book is applicable to proton–nucleus collisions, as we saw in Chapter 8. One can therefore test the predictions made in that chapter: in particular we showed that saturation physics predicts a transition of the nuclear modification factor from

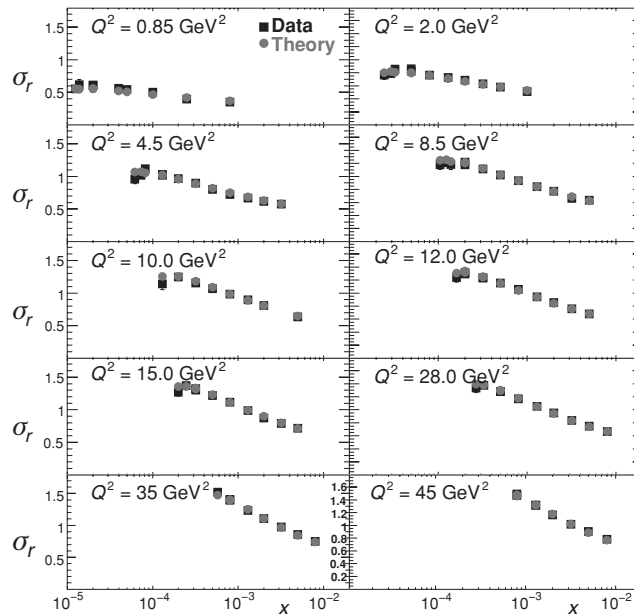


Fig. 9.3. Experimental data for the reduced DIS cross section (squares) in different Q^2 bins with, for comparison, the calculations of Albacete *et al.* (2011) (circles). The data are taken from the H1 and ZEUS collaboration (2010). (With kind permission from Springer Science+Business Media: Albacete *et al.* (2011).) A color version of this figure is available online at www.cambridge.org/9780521112574.

Cronin enhancement to suppression at all produced particle momenta p_T (see Fig. 8.11). This prediction may be compared with the data by means of Fig. 9.4, where we plot the nuclear modification factor R_{d+Au} for negatively charged hadrons obtained in deuteron–gold ($d+Au$) collisions at the Relativistic Heavy Ion Collider (RHIC) at Brookhaven National Laboratory by the BRAHMS collaboration. (At RHIC, data was collected for $d+Au$ collisions instead of pA ; we assume that the deuteron is also a dilute parton system, not unlike the proton.) The various different panels in Fig. 9.4 correspond to different pseudo-rapidity values; clearly, suppression sets in as the rapidity η increases, in agreement with the saturation physics prediction.

For dilute–dilute parton-system scattering (say, for pp collisions), we expect that two jets with large transverse momenta $\vec{p}_{1\perp}$ and $\vec{p}_{2\perp}$ are produced back to back, so that $\vec{p}_{2\perp} \approx -\vec{p}_{1\perp}$ as required by momentum conservation if we assume that the other produced particles are few and carry small transverse momenta. In the saturation phase, new processes are possible in which the large value of $\vec{p}_{1\perp}$ is not compensated by a single second jet but instead the momentum is distributed among many particles with average transverse momentum of order Q_s , thus depleting the back-to-back correlation of the jets. A large rapidity interval between the two measured particles only makes this effect stronger, by enhancing extra emissions by powers of rapidity. Figure 9.5 demonstrates that it is likely that this effect has been observed experimentally. Data on neutral pion correlations reported by the PHENIX

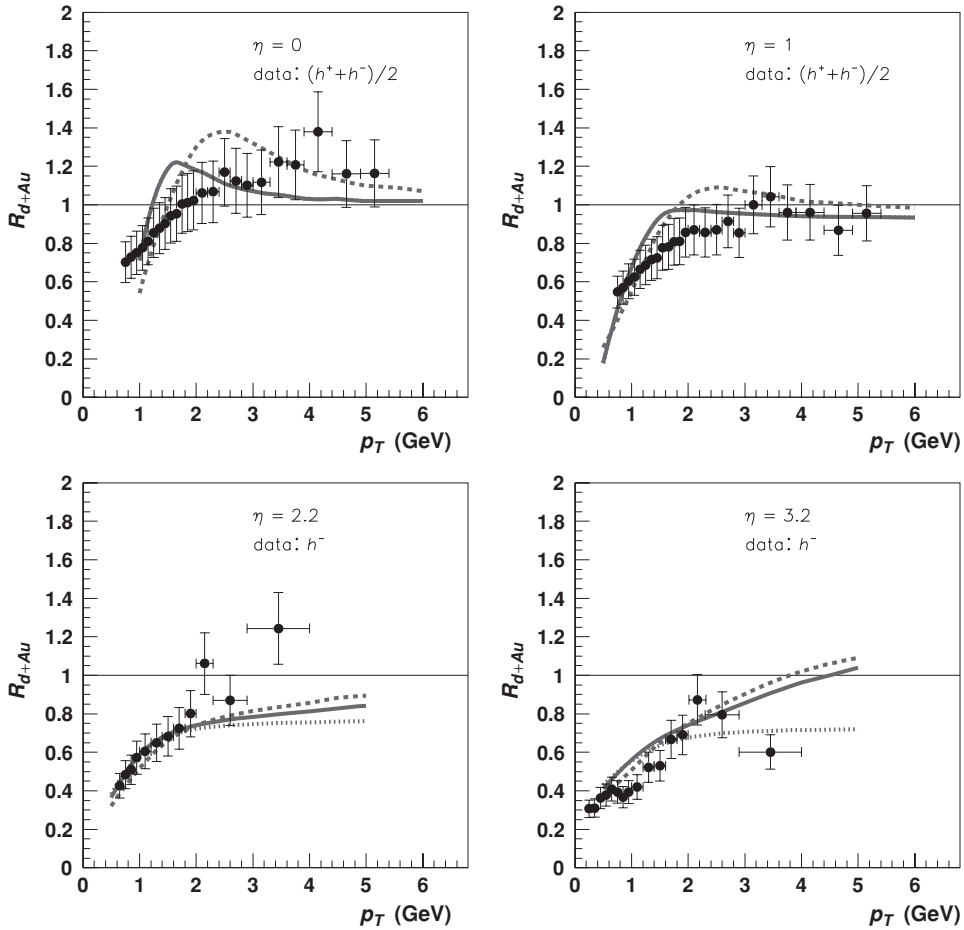


Fig. 9.4. Nuclear modification factor R_{d+Au} of charged particles for different pseudorapidities. The data are taken from the BRAHMS collaboration (2004). The theoretical curves and figures are taken from Kharzeev, Kovchegov, and Tuchin (2004). (Reprinted from Kharzeev, Kovchegov and Tuchin (2004), with permission from Elsevier.) A color version of this figure is available online at www.cambridge.org/9780521112574.

collaboration at RHIC are shown. The figure gives the $\pi^0-\pi^0$ correlation function for pp , $d+Au$ peripheral, and $d+Au$ central collisions as a function of the azimuthal angle $\Delta\phi$ between the pions (the angle in the transverse plane) for three different pairs of values of the pions' transverse momenta. One clearly sees that the back-to-back correlation at $\Delta\phi = \pi$ in the central $d+Au$ collisions, where saturation effects should be strongest, is indeed depleted as compared with the pp or peripheral $d+Au$ cases.

9.1.3 Proton–proton and heavy ion collisions

Proton–(anti)proton and nucleus–nucleus collisions are indeed very different in the sizes of the colliding particles and in the multiplicity of the produced particles. Still, saturation

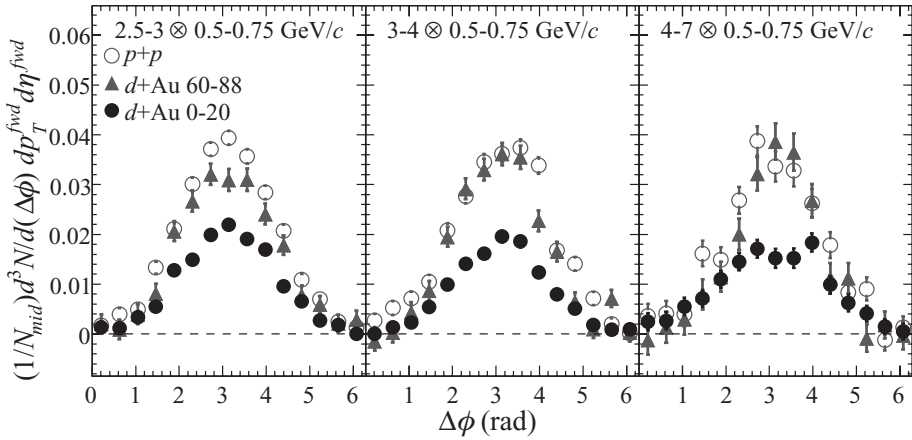


Fig. 9.5. The π^0 – π^0 correlation function for pp , $d+Au$ peripheral (60%–88% centrality) and $d+Au$ central (0%–20% centrality) collisions at $\sqrt{s_{NN}} = 200$ GeV, as a function of the azimuthal angle between the pions. The triggered π^0 is measured at mid-rapidity ($|\eta| < 0.35$), while the associated π^0 is at forward rapidity ($3.0 < |\eta| < 3.8$, deuteron direction). The transverse momenta of the triggered and associated pions are labeled at the top of each panel. (Reprinted with permission from the PHENIX collaboration (2011). Copyright 2011 by the American Physical Society.) A color version of this figure is available online at www.cambridge.org/9780521112574.

physics teaches us that at very high energies, when the saturation scales of the protons are large, pp collisions may start resembling AA collisions. While such a regime has not yet been accessed by modern-day accelerators, there are indications that it may be achieved at higher energies, and this led us to group those two reactions under one heading. These days, pp collisions are performed at the Large Hadron Collider (LHC) at CERN with the goal of finding the Higgs boson or particles outside the Standard Model of particle physics. Ultrarelativistic heavy ion (AA) collisions are being carried out at RHIC and LHC with the aim of creating a thermal medium of quarks and gluons, the quark–gluon plasma (QGP), and studying its properties (see e.g. the review by Kolb and Heinz (2003)).

The first piece of evidence in favor of saturation physics comes again from geometric scaling: one might expect that geometric scaling in the distribution functions would translate into such a scaling for the produced particle spectra; this conclusion is supported by more detailed calculations. Geometric scaling is observed in both pp and AA collisions and is depicted here in Fig. 9.6, where we show plots of charged-hadron transverse momentum spectra in pp and AA collisions as functions of the scaling variable $\tau = (p_T/Q_s)^{2+\lambda}$, where $Q_s = Q_0^{2/(2+\lambda)}(\sqrt{s} \times 10^{-3})^{\lambda/(2+\lambda)}$ with $Q_0 = 1$ GeV, \sqrt{s} measured in GeV, and λ as specified in the figures. In the AA case the scaling variable τ also includes a factor $A^{-1/3}$. The quality of scaling is much lower in the AA case owing to the quark–gluon plasma (QGP) final-state effects.

Since the saturation scale is the only relevant momentum scale in the problem, the hadron multiplicity produced in a pp or AA collision per unit transverse area should be

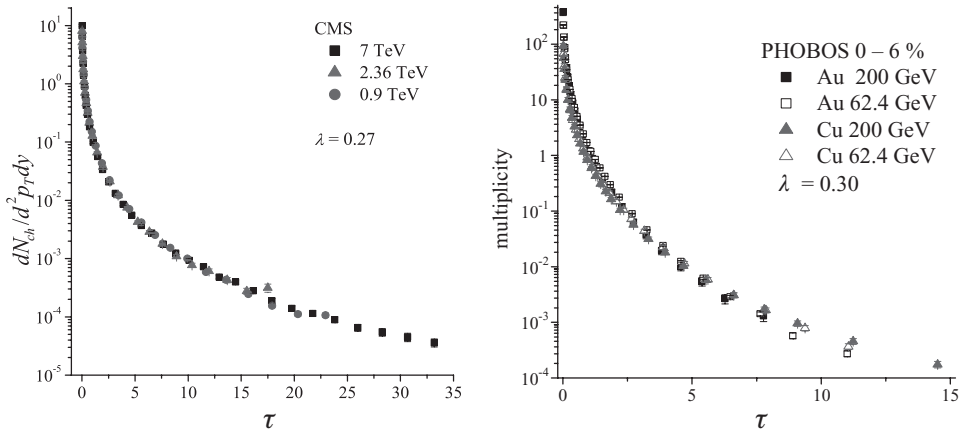


Fig. 9.6. Geometric scaling behavior of the charged hadron spectrum $dN_{ch}/d^2 p_T dy$ for proton–proton (left-hand panel) and heavy ion collisions (right-hand panel), plotted as a function of the scaling variable $\tau = (p_T/Q_s)^{2+\lambda}$ for several values of the center-of-mass energy. (Reprinted from McLerran and Praszalowicz (2011) (left) and Praszalowicz (2011) (right), with permission by *Acta Physica Polonica*. The data are as reported by the CMS collaboration (2010a, b) and the PHOBOS collaboration (2002, 2003) respectively. A color version of this figure is available online at www.cambridge.org/9780521112574.

proportional to the saturation scale squared (Gribov, Levin, and Ryskin 1983, McLerran and Venugopalan 1994a),

$$\frac{1}{S_{\perp}} \frac{dN}{dy} \sim Q_s^2, \tag{9.2}$$

leading to the prediction that the particle multiplicity should grow with Q_s^2 as a power of energy. A compilation of the experimental data on the hadron multiplicity in pp and AA collisions at various energies is shown in Fig. 9.7, demonstrating a power-of-energy growth for both reactions, along with saturation-model fits by Levin and Rezaeian (2011). (The highest-energy pp data point appeared after the saturation prediction.)

Saturation physics also predicts that the average transverse momentum of the produced particles should be proportional to the saturation scale, $\langle p_T \rangle \sim Q_s$ (see e.g. Fig. 8.7) since again it is the only scale in the problem. One expects $\langle p_T \rangle$ to grow with energy and, because of Eq. (9.2), with particle multiplicity. This behavior is demonstrated in Fig. 9.8. The left-hand panel of Fig. 9.8 shows a compilation of the proton–proton and proton–anti-proton collision data collected in several experiments over the years, demonstrating that $\langle p_T \rangle$ does grow with energy. The right-hand panel of Fig. 9.8 shows the growth of $\langle p_T \rangle$ with charged-hadron multiplicity in pp collisions at LHC. It should be stressed that, in the traditional approaches based on high energy pomeron phenomenology, $\langle p_T \rangle$ does not depend on either energy or multiplicity; therefore we consider the observation of these dependences in Fig. 9.8 as a strong argument in favor of the advantage of saturation physics over such models.

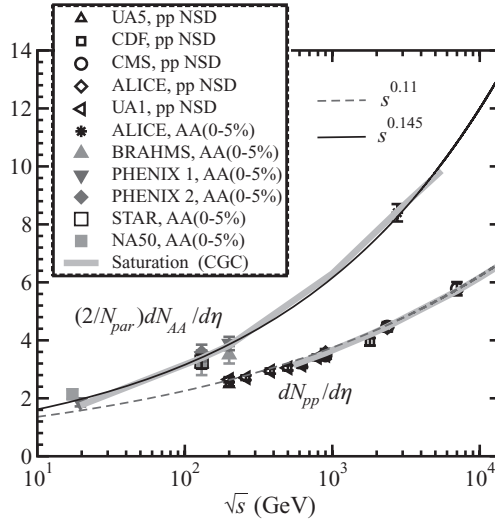


Fig. 9.7. Dependence of hadron multiplicity on energy for *pp* (lower curve and points) and *AA* (upper curve and points) collisions. (Reprinted with permission from Levin and Rezaeian (2011). Copyright 2011 by the American Physical Society.) A color version of this figure is available online at www.cambridge.org/9780521112574.

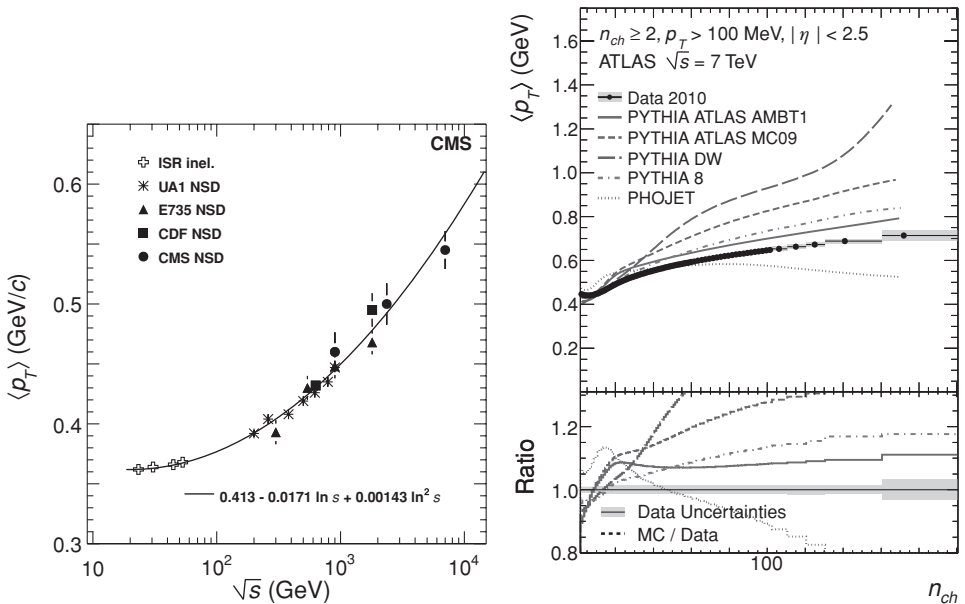


Fig. 9.8. Dependence of the average transverse momentum on energy (left-hand panel) and on multiplicity and hence on centrality (right-hand panel). (The left-hand panel is reprinted with permission from the CMS collaboration (2010b). Copyright 2010 by the American Physical Society. The right-hand panel is reprinted from the ATLAS collaboration (2011), with permission by IOP Publishing.) A color version of this figure is available online at www.cambridge.org/9780521112574.

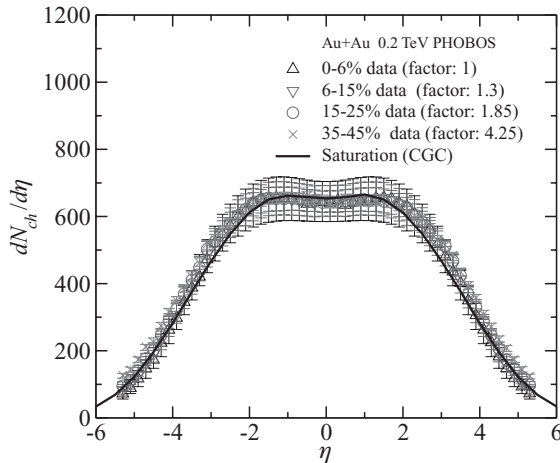


Fig. 9.9. Dependence of hadron multiplicity on rapidity for AA collisions. The experimental data are from the PHOBOS collaboration at RHIC (see PHOBOS collaboration, 2002, 2003). (Reprinted with permission from Levin and Rezaeian (2011). Copyright 2011 by the American Physical Society.) A color version of this figure is available online at www.cambridge.org/9780521112574.

It is difficult to make precise quantitative saturation/CGC physics predictions for the hadron multiplicity and spectra in pp and AA collisions since, mentioned above, these theoretical problems have not been solved. Instead, as a reasonable approximation to the full answer, one may use the k_T -factorization formula (8.45) with the q_T -integral cut off by an upper bound proportional to k_T . This is known as the Kharzeev–Levin–Nardi (KLN) approach (Kharzeev and Nardi 2001, Kharzeev and Levin 2001, Kharzeev, Levin, and Nardi 2005a, b). Predictions based on the KLN approach have been quite successful in describing heavy ion data on multiplicities. A fit of the RHIC multiplicity data plotted as a function of pseudo-rapidity for different centrality bins (denoted by percentages in the legend, along with the appropriate scaling factors) based on the KLN model is shown in Fig. 9.9; clearly the data is well described by the saturation model.

This agreement between the multiplicity data in heavy ion collisions and the saturation predictions is further illustrated in Fig. 9.10, where we show the particle multiplicity per participating nucleon as a function of the collision centrality; N_{part} is the number of nucleons participating in the collision and varies between a few for peripheral collisions to $2A$ for central collisions (for identical nuclei). The three lower lines in the legend of Fig. 9.10 correspond to *predictions* coming from saturation-based models.¹ Clearly all the curves do well; the prediction by Albacete and Dumitru (2011) (the short-dashed curve in Fig. 9.10) based on rcBK evolution for the dipole amplitude combined with the KLN model for particle production matches the data almost perfectly.

¹ The three upper curves in the legend of Fig. 9.10 are Monte-Carlo simulations not based on saturation physics; note, however, that the HIJING event generator prediction uses an IR cutoff that grows with energy, which is reminiscent of the saturation scale.

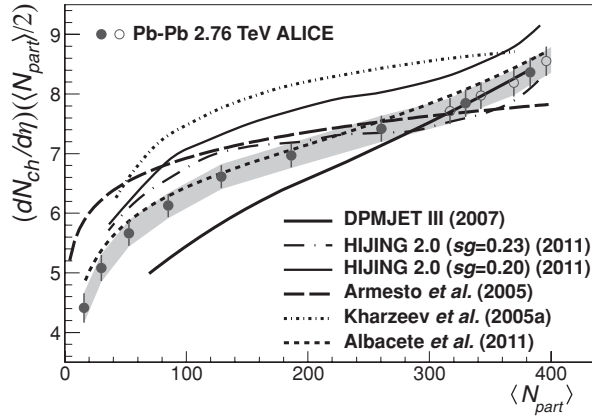


Fig. 9.10. Dependence of hadron multiplicity on collision centrality for AA collisions: the saturation-based models are from Armesto *et al.* (2005), Kharzeev *et al.* (2005a), and Albacete *et al.* (2011), while the no-saturation Monte-Carlo simulations are DPMJET III, Bopp *et al.* (2007); HIJING, Deng *et al.* (2011). (Reprinted with permission from the ALICE collaboration (2011) at the LHC. Copyright 2011 by the American Physical Society.) A color version of this figure is available online at www.cambridge.org/9780521112574.

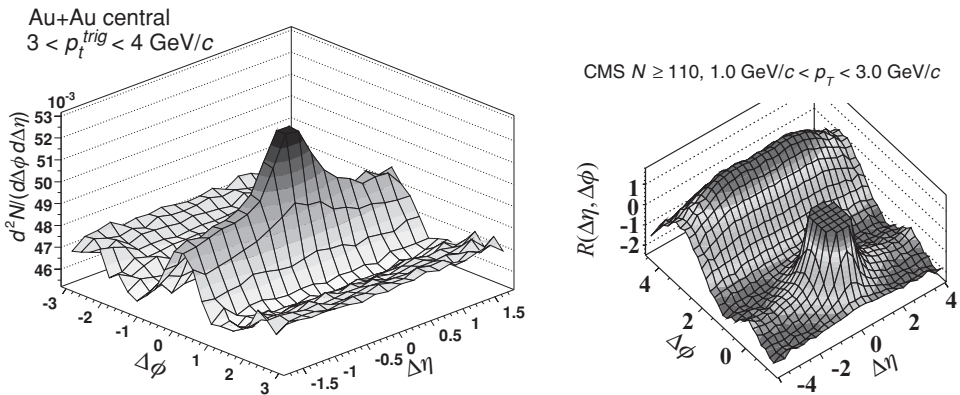


Fig. 9.11. Two-particle correlation function plotted versus pseudo-rapidity interval $\Delta\eta$ and azimuthal angle $\Delta\phi$ between the particles for AA (left-hand panel) and high-multiplicity pp (right-hand panel) collisions. (Left-hand panel: reprinted figure with permission from the STAR collaboration (2009). Copyright 2009 by the American Physical Society. Right-hand panel: reprinted with kind permission from Springer Science+Business Media: CMS collaboration (2010a).) A color version of this figure is available online at www.cambridge.org/9780521112574.

Another possible piece of evidence in favor of saturation/CGC physics is provided by the long-range rapidity correlations between the produced hadrons at small azimuthal angles $\Delta\phi \approx 0$, which have been seen in AA and, more recently, in pp collisions and are shown in Fig. 9.11. Owing to the shape of these correlations they are often referred to as the “ridge”. The search for a detailed explanation of them in the saturation framework is still

in progress (see Gavin, McLerran, and Moschelli (2009), and Dumitru *et al.* 2008, 2011a, b), but a discussion of this work is beyond of the scope of the present text. However, two facts, inherent properties of the saturation approach, are shown experimentally. First, the correlations are long-range in rapidity. Second, in pp collisions the long-range rapidity correlations at $\Delta\phi \approx 0$ appear only in events with high multiplicity ($N \geq 110$ in the right-hand panel of Fig. 9.11): hence high-multiplicity pp collisions appear to be similar to the AA collisions. This suggests that the source of the correlations shown in Fig. 9.11 is in the properties of dense parton systems.

9.2 Unsolved theoretical problems

In this book we have tried to introduce our readers to the new world of the ideas and methods of high energy QCD. We hope that after reading our book the reader will be able to work in this field, which is in the early stages of development. We conclude the book by outlining unsolved theoretical problems in the field.

1. Impact parameter dependence In Chapters 4 and 5 we showed that the dipole–nucleus forward scattering amplitude $N(\vec{x}_\perp, \vec{b}_\perp, Y)$ resulting either from the GGM model or from BK/JIMWLK evolution does not violate the black-disk limit, so that one always has $N \leq 1$. While this is an improvement over BFKL evolution, some unitarity problems still remain. As we saw in Sec. 3.3.6, the Froissart–Martin bound consists of two ingredients, that the scattering obeys the black-disk limit and that the radius of the black disk grows logarithmically with energy. As follows from Eq. (3.115), the latter property results from QCD having a mass gap (since the lightest particle in the spectrum, the pion, has a nonzero mass). In perturbative QCD one works with gluons, which have zero mass: clearly Eq. (3.115) should no longer apply and the Froissart–Martin bound is violated.

To see this explicitly imagine that we are trying to prove the Froissart–Martin bound for onium–onium scattering. Consider the scattering at large impact parameter b_\perp , where the scattering amplitude is small and nonlinear saturation corrections can be neglected. The onium–onium scattering cross section, defined in Eq. (4.85), is then governed by the BFKL evolution (4.87) (in the LLA). At large b_\perp one can show that the general BFKL equation solution in Eq. (4.126) leads to

$$n(\vec{x}_{10}, \vec{x}_{1'0'}, \vec{b}_\perp, Y) \xrightarrow{b_\perp \gg x_{10}, x_{1'0'}} \int_{-\infty}^{\infty} d\nu \left(\frac{x_{10}^2 x_{1'0'}^2}{b_\perp^4} \right)^{1/2+i\nu} C(\nu) e^{\bar{\alpha}_s \chi(0, \nu) Y}, \tag{9.3}$$

where $C(\nu)$ is a function of ν , the exact form of which is not important to us. Evaluating the ν -integral in Eq. (9.3) near the saddle point at $\nu = 0$, we get

$$n(\vec{x}_{10}, \vec{x}_{1'0'}, \vec{b}_\perp, Y) \xrightarrow{b_\perp \gg x_{10}, x_{1'0'}} \frac{x_{10} x_{1'0'}}{b_\perp^2} e^{(\alpha_p - 1)Y}. \tag{9.4}$$

Using Eq. (9.4) instead of Eq. (3.113), we obtain the black-disk radius $R = b^*$ by requiring that (cf. Eq. (3.114))

$$\frac{x_{10} x_{1'0'}}{b^{*2}} e^{(\alpha_P - 1)Y} \propto 1 \quad (9.5)$$

so that

$$b^{*2} \propto s^{\alpha_P - 1}. \quad (9.6)$$

Thus the radius of interaction increases as a power of s , $R^2 \sim s^{\alpha_P - 1}$. The total cross section increases as a power of energy too,

$$\sigma_{tot} = 2\pi R^2 \propto s^{\alpha_P - 1}. \quad (9.7)$$

We conclude that nonlinear evolution gives a scattering amplitude that satisfies the black-disk limit but still leads to a violation of the Froissart–Martin bound, owing to the fast growth of the black disk.

This power-like increase in the total cross section was first discussed by Kovner and Wiedemann (2002a, b, 2003). Their conclusions were confirmed by a numerical solution of the BK equation with impact parameter dependence performed by Golec-Biernat and Stasto (2003) (see also Gotsman *et al.* (2004)). Equation (9.7) shows that saturation/CGC physics (or any other perturbative QCD calculation) cannot be trusted in large-impact-parameter scattering and some nonperturbative effects need to come in to make the total cross section satisfy the Froissart–Martin bound. One hopes that, with some minimalistic assumptions about confinement physics included in the evolution, and for a large nucleus, such peripheral nonperturbative effects would give a relatively small contribution to the total cross section, since the perimeter scales as a smaller power of A than the area. The existing data appears to indicate that such a hope is not unfounded.

2. Higher-order corrections to the BFKL, BK, and JIMWLK evolution equations

We have briefly discussed the problem of higher-order corrections to the BFKL evolution in Sec. 6.3, outlining possible ways of getting the corrections under control. To improve the precision of the BK/JIMWLK predictions for the phenomenology, one needs to carry out this (or any other) program for calculating higher-order corrections to these nonlinear evolution equations. Would the agreement with the data shown in Sec. 9.1 survive the inclusion of higher-order corrections? Can we devise a systematic way of improving the precision of the nonlinear evolution equations? These are important questions, which need to be studied seriously.

3. Scattering of two dilute systems: BFKL pomeron loops At first sight the scattering of one dilute system of partons on another dilute system of partons (say the scattering of two onia with small sizes) can be described by the exchange of a BFKL pomeron. However, as we discussed in Sec. 3.3.6, such a contribution would violate the black-disk limit at high energy. Owing to the low initial parton density in both onia (so that there is no parameter A), the pomeron fan diagrams of Fig. 3.23 in such a dilute–dilute scattering are not enhanced compared to the pomeron loop diagrams of Fig. 3.24: both kinds of interaction have to be included. The BK/JIMWLK evolution equations assume that one

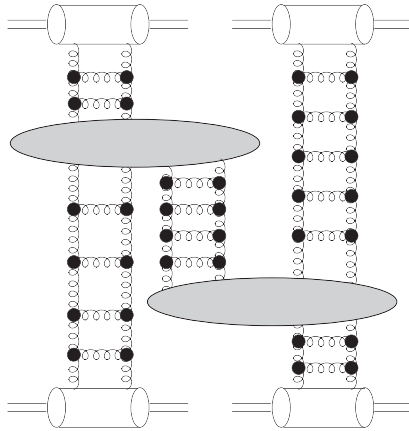


Fig. 9.12. A diagram contributing to the total cross section of nucleus–nucleus scattering in the BFKL pomeron calculus.

scattering particle (the nucleus) is large and thus do not contain the pomeron loop contributions from Fig. 3.24. Nonetheless it is likely that such contributions are essential for the unitarization of onium–onium scattering. This problem is important because the high energy onium–onium scattering process will happen in the next-generation linear colliders (where each colliding lepton could split into a virtual photon, with each γ^* in turn splitting into a $q\bar{q}$ pair). On top of that, unitarization in a dilute–dilute scattering would be “pure QCD” in its nature, since it would not be relying on a large nucleus as one of the scatterers. In spite of many efforts (see Salam 1995, 1996, Navelet and Peschanski 1999, Mueller, Shoshi, and Wong 2005, Levin and Lublinsky 2005b, Iancu and Triantafyllopoulos 2005, Kovner and Lublinsky 2005d, Hatta *et al.* 2006, Altinoluk *et al.* 2009, Levin, Miller, and Prygarin 2008) we are still far from understanding this problem of dilute–dilute scattering.

4. Heavy ion collisions We have already mentioned, in Sec. 8.3, that the calculation of gluon and quark production in AA collisions in the saturation/CGC framework is an important problem for understanding the early-time dynamics of heavy ion collisions. While some progress on this issue has been achieved lately, mainly along the lines of finding a numerical solution, the problem is still an open one. A related problem, which is also open, is the problem of thermalization in heavy ion collisions: one needs to understand how the produced quarks and gluons form a thermal medium (QGP), which is likely to be observed in heavy ion collisions.

Multi-particle correlations in AA collisions are also important, particularly correlations in rapidity since they are sensitive to subtle details of the early-time dynamics and can be measured experimentally. Initial progress on this issue has recently been achieved by Gavin, McLerran, and Moschelli (2009), and by Dumitru *et al.* (2008, 2011a, b).

Another, related, unsolved theoretical problem concerns the calculation of the total nucleus–nucleus scattering cross section in the saturation/CGC framework. One has to sum diagrams fanning out in the directions of both nuclei (Braun 2000b, 2004). A sample

diagram contributing to this process is shown in Fig. 9.12. An equation summing all such diagrams has been suggested by Braun (2000a, 2004) using the BFKL pomeron calculus. The solution of such an equation is not known, however, and it is yet to be reproduced using the BK/JIMWLK approach (see Altinoluk *et al.* (2009)).

Further reading

The inevitable space limitations of this book did not allow us to include (or do justice to) everything that is known about high energy QCD. We had to make a selection based on what, in our opinion, is needed to quickly bring a student or a researcher from a neighboring field up to speed in saturation/CGC physics. Below, some topics that did not make it into the book are introduced briefly; they constitute our final recommendation for further reading, complementary to all our earlier suggestions.

Ciafaloni (1988), Catani, Fiorani, and Marchesini (1990a, b), and Marchesini (1995) suggested an evolution equation that, in the framework of a single equation, reproduces both the Q^2 (DGLAP) and x (BFKL) evolutions. This result, known as the CCFM equation, is at the foundation of most Monte Carlo simulations of high energy collisions. While the presentation of CCFM goes beyond the scope of this book, we certainly recommend our readers to learn more about this equation by reading the original papers mentioned above.

We have also omitted any presentation of particle production in the collinear factorization framework; however, the reader may learn the basics of collinear factorization from the textbook by Sterman (1993), with more advanced results along with a presentation of the related jet physics given by Dokshitzer, Diakonov, and Troian (1980), Collins, Soper, and Sterman (1985a, b, 1988a, b), Dokshitzer *et al.* (1991), and Collins (2011).

Finally, in our book we have presented only the basic aspects of the connections between saturation/CGC physics and heavy ion collisions. This is in part due to the fact that understanding AA collisions in saturation physics is a difficult, unsolved, problem. We recommend the reviews by McLerran (2005, 2008, 2009a) as a starting point for the further exploration of the richness of the saturation/CGC dynamics in AA collisions.